Fast-dissolving electrospun gelatin nanofibers encapsulating ciprofloxacin/cyclodextrin inclusion complex

Zeynep Aytac[a], Semran Ipek[a,b], Ismail Erol[c], Engin Durgun[a,d,*], Tamer Uyar[a,e,**]

[a] Institute of Materials Science & Nanotechnology, Bilkent University, Ankara, 06800, Turkey
[b] Department of Engineering Physics, Istanbul Medeniyet University, Istanbul 34700, Turkey
[c] Department of Chemistry, Gebze Technical University, Kocaeli, 41400, Turkey
[d] UNAM-National Nanotechnology Research Center, Bilkent University, Ankara, 06800, Turkey
[e] Department of Fiber Science and Apparel Design, College of Human Ecology, Cornell University, Ithaca, NY, 14853, USA

ABSTRACT

Electrospun gelatin nanofibrous matrix encapsulating ciprofloxacin (CIP)/hydroxypropyl-beta-cyclodextrin (HPβCD)-inclusion complex (IC) was produced via electrospinning method. Computational modeling indicated that van der Waals forces are the most significant driving forces for the complexation and hydrophobic moiety (piperazinyl) of CIP, which was included in the cavity of HPβCD. The FTIR and XRD studies indicated the formation of CIP/HPβCD host/guest complexation, FTIR also suggested that hydrophobic moiety of CIP is in the HPβCD cavity in parallel with the computational modeling results. The phase solubility diagram demonstrated that the solubility of CIP was enhanced after complexation with HPβCD. SEM images showed that electrospun gelatin nanofibers encapsulating CIP/HPβCD-IC have bead-free morphology with a diameter of ˜90 nm. The gelatin nanofibrous mat loaded with CIP/HPβCD-IC has exhibited fast-dissolving character in water compared to gelatin/CIP nanofibrous mat due to the enhanced wettability of the nanofibrous mat by HPβCD and improvement achieved in the solubility of CIP.

1. Introduction

Electrospinning is one of the most widely used method to produce polymeric nanofibers [1]. Simplicity and universality of the technique enables nanofibers to be used in the areas such as drug delivery and wound dressing by adding bioactive molecules including antibiotics, antibacterial agents, flavor/fragrances, and antioxidants [2–4]. High surface area to volume ratio, nano-scale diameter, and porous structure of electrospun nanofibers provides unique properties to the system. In line with the novelty that our group brought to the literature, cyclodextrin (CD) inclusion complexes (ICs) of the bioactive molecules were encapsulated in electrospun nanofibers [5–14]. CDs (Fig. 1a–b) are non-toxic cyclic oligosaccharides capable of forming ICs with various guest molecules having appropriate polarity and dimension owing to the hydrophobic cavity of the host molecule (i.e. hydroxypropyl-beta-cyclodextrin (HPβCD)) [15]. Weak forces such as van der Waals interactions, electrostatic interactions, and hydrogen bonding and water molecules residing in the cavity of CDs with high-enthalpy, are the main driving forces to form ICs [16,17]. CDs are not only used for research

purpose but also in the pharmaceutical industry to control the release, and to improve solubility, chemical stability, and bioavailability of the drugs [16,17].

Ciprofloxacin (CIP, 1-cyclopropyl-6-fluoro-1,4-dihydro-4-oxo-7-(1-piperazinyl)-3-quinoline carboxylic acid, Fig. 1c) is an antibiotic which was used in the form of IC in the literature with various types of CDs. It is a known fact that α-CD, β-CD, and γ-CD are the most commonly used native CDs for a variety of guest molecules. Several studies were reported by using CIP and native [18–20] or modified CDs, in which some hydroxyl groups of β-CD were replaced with hydroxypropyl or methyl groups such as hydroxypropyl-beta-cyclodextrin (HPβCD) and methylated-beta-cyclodextrin (MβCD) [21,22]. Masoumi et al. produced electrospun polycaprolactone (PCL) nanofibers loaded with IC of CIP and two native CDs, α-CD and β-CD. It was also shown that the release of CIP was improved with complexation due to the solubility increment in the drug [23].

On the other hand, there are also studies in the literature using electrospun nanofibers as fast dissolving drug delivery systems. Illangakoon et al. produced nanofibers of polyvinylpyrrolidone (PVP)
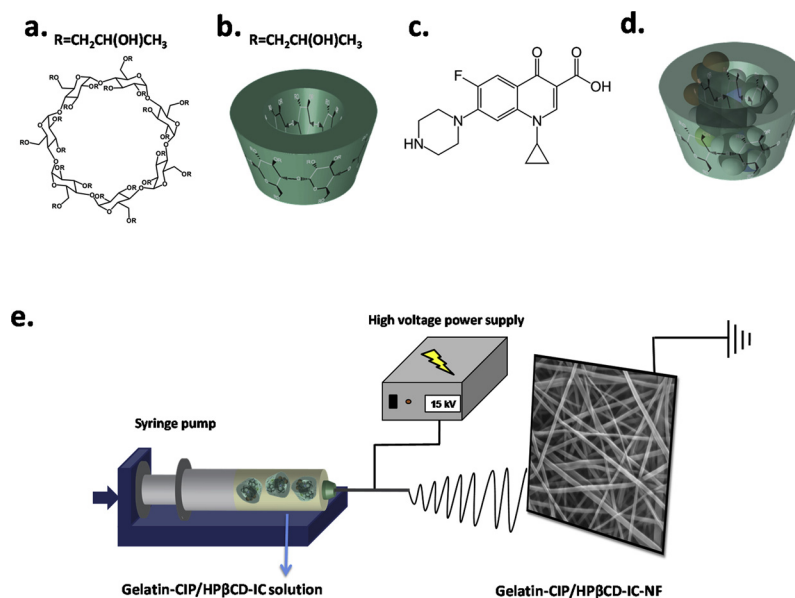

Fig. 1. (a) The chemical structure of HPβCD, (b) schematic representation of HPβCD, (c) the chemical structure of CIP, (d) schematic representation of CIP/HPβCD-IC formation, and (e) electrospinning of nanofibers from gelatin-CIP/HPβCD-IC solution.

loaded with paracetamol/caffeine [24]. Similarly, Wu et al. developed core-shell nanofibers having helicid in the core. Here, sucralose was used in the shell to mask the bitter taste of helicid [25]. Furthermore, CDs were also used to obtain fast dissolving nanofibers. In the studies of Samprasit et al., CD-ICs of drugs were encapsulated in the electrospun nanofibers to improve the stability of the nanofibrous mats and provide less bitter taste of the drug as a fast dissolving system as compared to drug encapsulated in powder form [26,27].

In this study, gelatin nanofibers encapsulating CIP/HPβCD-IC (Fig. 1d) were obtained using electrospinning technique. After the confirmation of CD-IC formation by computational modeling and experimental studies including phase solubility, ^{1}H-NMR, FTIR, XRD, and TGA, CIP/HPβCD-IC were encapsulated into gelatin nanofibers (Fig. 1e) to facilitate the application of CIP/HPβCD-IC as a drug delivery system. Only CIP encapsulated gelatin nanofibers were produced as a reference. Then, the morphology of nanofibers was checked by SEM. XRD and TGA were also employed for the further characterization of the nanofibers. Finally, dissolution studies were performed for both nanofibers to show the change in the dissolution behavior of nanofibers depending on the added molecule, either CIP or CIP/HPβCD-IC.

2. Experimental

2.1. Materials

Gelatin (from porcine skin, gel strength 300, Type A, Sigma-Aldrich), ciprofloxacin (CIP, ≥98%, Fluka), acetic acid (AA, extra pure 100%, Sigma Aldrich), and deuterated dimethyl sulfoxide (DMSO-d6, deuteration degree min 99.8% for NMR spectroscopy, Merck) were purchased and used as received without any further purification. Hydroxypropyl-beta-cyclodextrin (HPβCD, degree of substitution ~ 0.6) was gift from Wacker Chemie AG (Germany). The water was distilled-deionized from a Millipore Milli-Q ultrapure water system.

2.2. Preparation of the ciprofloxacin/cyclodextrin inclusion complex (CIP/HPβCD-IC)

CIP/HPβCD-IC (1:1) was synthesized according to the freeze-drying method. Firstly, 0.23 g CIP was added to 2 mL of aqueous solution of HPβCD (1 g) at 1:1 ratio. The solution was stirred for 12 h at room temperature (RT). Finally, CIP/HPβCD-IC (1:1) powder was obtained

after the solution was lyophilized for 5 days.

2.3. Preparation of electrospinning solutions

Gelatin nanofibers without CIP, with only CIP, and with CIP/HPβCD-IC were all produced via electrospinning method (gelatin-NF, gelatin-CIP-NF, and gelatin-CIP/HPβCD-IC-NF). Gelatin-CIP/HPβCD-IC-NF was produced by adding certain amount of CIP/HPβCD-IC which contains 10% CIP (w/w, with respect to gelatin) into 13% gelatin (w/v) solution prepared in 2 mL of water/AA (7/3, v/v) at RT in 1 h. Reference samples (gelatin-NF and gelatin-CIP-NF) were prepared by using 13% gelatin (w/v) dissolved in water/AA (7/3) at RT for 1 h. For gelatin-CIP-NF, 10% CIP (w/w, with respect to gelatin) was added into the gelatin solution. Table S1 summarizes the composition of the gelatin, gelatin-CIP, and gelatin-CIP/HPβCD-IC solutions.

2.4. Electrospinning

3 mL plastic syringe (metallic needle: 0.9 mm diameter) was used to load 2 mL solutions prior to electrospinning. The solutions in the syringe were mounted on the syringe pump (WPI, SP 101IZ) and fed at a constant rate of 1 mL/h. Therefore, electrospinning of the solutions took 2 h in total. In the meantime, high voltage power supply (AU Series, Matsusada Precision Inc.) was used to apply 15 kV. Nanofibers were collected on a grounded collector, which is at 15 cm away from the needle tip, covered with a piece of aluminum foil. The experiments were performed at 25 °C and 18% relative humidity.

2.5. Characterizations and measurements

Solubility improvement of CIP in the form of IC with HPβCD was investigated by using phase solubility diagram. Excess amount of CIP was added into 0–6 mM of HPβCD dissolved in aqueous solution and the mixtures were filtrated after stirring them for 24 h. Finally, UV measurements were taken at 275 nm (Cary 100, Varian). The experiments were performed in triplicate (n = 3) and the results are reported as average ± standard deviation.

The proton nuclear magnetic resonance (^{1}H-NMR) spectra of CIP, HPβCD, and CIP/HPβCD-IC were recorded with Bruker DPX-400 after dissolving the powders in d6-DMSO. Since the solubility of CIP and CIP/HPβCD-IC (10 mg/mL) is quite low in d6-DMSO, these solutions

were filtrated after the incubating them at RT for 12 h. The integration of the chemical shifts (δ) given in parts per million (ppm) were calculated by Mestrenova software. Then, the molar ratio of CIP:HPβCD was decided.

The pellets of CIP, HPβCD, and CIP/HPβCD-IC for Fourier transform infrared spectrometer (FTIR) measurement were obtained by mixing the powder of the as-received CIP and HPβCD, and previously synthesized CIP/HPβCD-IC samples with potassium bromide (KBr). Then, infrared spectra were scanned 64 times for each sample between 4000 cm^{-1} and 400 cm^{-1} at a resolution of 4 cm^{-1} (Bruker-VERTEX 70).

The crystalline structure of powder of CIP, HPβCD, and CIP/HPβCD-IC; and gelatin-NF, gelatin-CIP-NF, and gelatin-CIP/HPβCD-IC-NF were detected by X-ray diffraction (XRD, PANalytical X'Pert powder diffractometer) in a 2θ range of 5°–30°.

Thermal properties of CIP, HPβCD, CIP/HPβCD-IC, gelatin-NF, gelatin-CIP-NF, and gelatin-CIP/HPβCD-IC-NF were characterized by thermal gravimetric analysis (TGA, TA Q500, USA). TGA was performed at a heating rate of 20 °C/min from 25 °C to 500 °C for CIP, HPβCD, CIP/HPβCD-IC and 600 °C for gelatin-NF, gelatin-CIP-NF, and gelatin-CIP/HPβCD-IC-NF under the flow of nitrogen.

Morphological characterization of nanofibers was performed by scanning electron microscopy (SEM, FEI-Quanta 200 FEG). The SEM samples of nanofibers were prepared by mounting nanofibers on SEM stubs with a double-sided copper tape and then sputter-coated with Au/Pd layer, which is 5 nm (PECS-682). The average fiber diameter (AFD) of nanofibers were calculated from the SEM images (n = 100) and the fiber diameters were reported as the average ± standard deviation.

The dissolution of gelatin-CIP-NF and gelatin-CIP/HPβCD-IC-NF were demonstrated by immersing 10 mg of nanofibers in 30 mL water. During the immersion, the photographs of the petri dishes, in which nanofibers were immersed, were taken at 5, 120, and 1440 min. Videos were also recorded for both nanofibers up to 45 s of immersion.

2.6. Computational method

2.6.1. Molecular docking simulations

The 3D coordinates of CIP were retrieved from the Drugbank database with the accession number DB00537 (https://www.drugbank.ca/drugs/DB00537). To obtain rational conformations of the 1:1 CIP/HPβCD-IC, molecular docking simulations were performed. In docking simulations, CIP was treated as ligand (guest) and CD was treated as receptor (host) molecule. AutoDock Tools software (version 1.5.6) was used to add polar hydrogen atoms, Gasteiger charges and set up rotatable bonds for both guest and host molecules [28]. CIP was docked to center of the binding cavity of the CD molecule using following Cartesian coordinates x = 9.819 Å, y = 11.785 Å, z = 11.145 Å. The grid spacing of 0.375 Å and grid dimension of 40 Å x 40 Å x 40 Å was used. Except genetic algorithm runs (ga_run) all settings were used as default. To increase CIP conformational sampling ga_run was set to 100. For molecular docking simulation analyses and visualization, AutoDock Tools [28], Pymol molecular graphics system (Schrödinger, LLC, San Diego, CA, USA) and UCSF Chimera package [29] were used.

2.6.2. Molecular dynamics simulations

The best docking pose with the highest binding energy was considered as the initial structure of CIP/HPβCD-IC consisting of HPβCD and CIP. This initial structure of CIP/HPβCD-IC was further subjected to molecular dynamics simulations. Charmm-gui input generator [30,31] was used to generate input files for molecular dynamics simulations, HPβCD and CIP were parametrized using CGenFF [32]. CIP/HPβCD-IC was first solvated with 5000 TIP3 type water molecules, and then neutralizing ions were added to the simulation box. The energy of the whole system (CIP-HBPCD and water molecules) was minimized using steepest descent algorithm for 500 ps, and subsequently subjected to NVT (constant volume and temperature) to reach equilibrium in energy

landscape at 303.15 K. In production run simulations NPT (constant pressure and temperature) ensemble was used. Classical MD run was performed for 30 ns without any constraints at 303.15 K by using CHARMM36 force field [32] and GROMACS package (version 5.0) [33]. Temperature was maintained using Nose-Hoover thermostat [34]. Particle Mesh Ewald (PME) method was applied for electrostatic interactions [35] and LINCS algorithm was used to constraint the intramolecular bond lengths [36].

Equilibrium properties, structure and dynamics of the systems were calculated over the 30 ns simulation runs after the systems were equilibrated for 500 ps. Moreover, we have used clustering algorithm to identify similar structures encountered during 30 ns MD trajectory with a 2 Å root-mean-square deviation (RMSD) cut-off.

2.6.3. Molecular mechanics-Poisson Boltzmann surface area (MM-PBSA) calculations

Poisson-Boltzmann or generalized Born and surface area continuum solvation method (MM-PBSA) was successfully applied to estimate the free energy of the binding (ΔG_{bind}) of CD-ICs [37]. Although this method involves several approximations and it is not accurate as much as other methods such as free energy perturbation (FEP) or thermodynamic integration (TI), it may be still useful to understand experimental trends. ΔG_{bind} of the CIP/HPβCD-IC was calculated by subtracting isolated CD and CIP free energies (ΔG_{CD} and ΔG_{CIP}) from free energy of complex ($\Delta G_{complex}$).

$$\Delta G_{bind} = \Delta G_{complex} - (\Delta G_{CD} + \Delta G_{CIP}) \tag{1}$$

The total Gibbs free energy (ΔG) can be calculated as follows;

$$\Delta G = \Delta E_{MM} - T\Delta S + \Delta G_{solv} \tag{2}$$

The change of entropy upon guest binding, -TΔS, was computed by normal-mode analysis on a set of conformational snapshots taken from MD simulations. T and S denote temperature and entropy, respectively. The TΔS contribution was calculated according to quasi harmonic approximation as implemented in Gromacs [33].

ΔEMM is the vacuum potential energy, and composed of bonded and nonbonded terms in gas phase (van der Waals and electrostatics) which are given as follows;

$$\Delta E_{MM} = \Delta E_{Bonded} + (\Delta E_{vdW} + \Delta E_{elec}) \tag{3}$$

Last term in (2) ΔG_{solv} represents required energy to transfer solute molecule from vacuum to solvent environment, and constituted by two terms; polar and nonpolar, as follows,

$$\Delta G_{solv} = \Delta G_{polar-solvation} + \Delta G_{nonpolar-solvation} \tag{4}$$

$$- TdS = \Delta G_{bind} - \Delta H \tag{5}$$

$$\Delta G_{bind} = RTlnK_{bind}$$

ΔG_{polar} is estimated by solving Poisson-Boltzmann equation, and $\Delta G_{nonpolar}$ is calculated by solvent accessible surface area (SASA) model [38].

3. Results and discussion

3.1. Computational modeling of CIP/HPβCD-IC

3.1.1. Docking results

The molecular docking process have been performed to determine the most preferred docking conformations for CIP within HPβCD cavity. The RMSD fluctuations less than 2.0 Å is used to cluster the structures. Clustering analysis of docking studies has resulted in two structures with lower mean binding free energy as given in Fig. 2a–b. CIP has been found to locate in HPβCD cavity with minor conformational differences in both docking poses gathered. CIP has only one hydrogen bond within HPβCD cavity for both structures with a bond length of 2.018 Å and 2.191 Å for a and b structures given in Fig. 2a–b, respectively. The
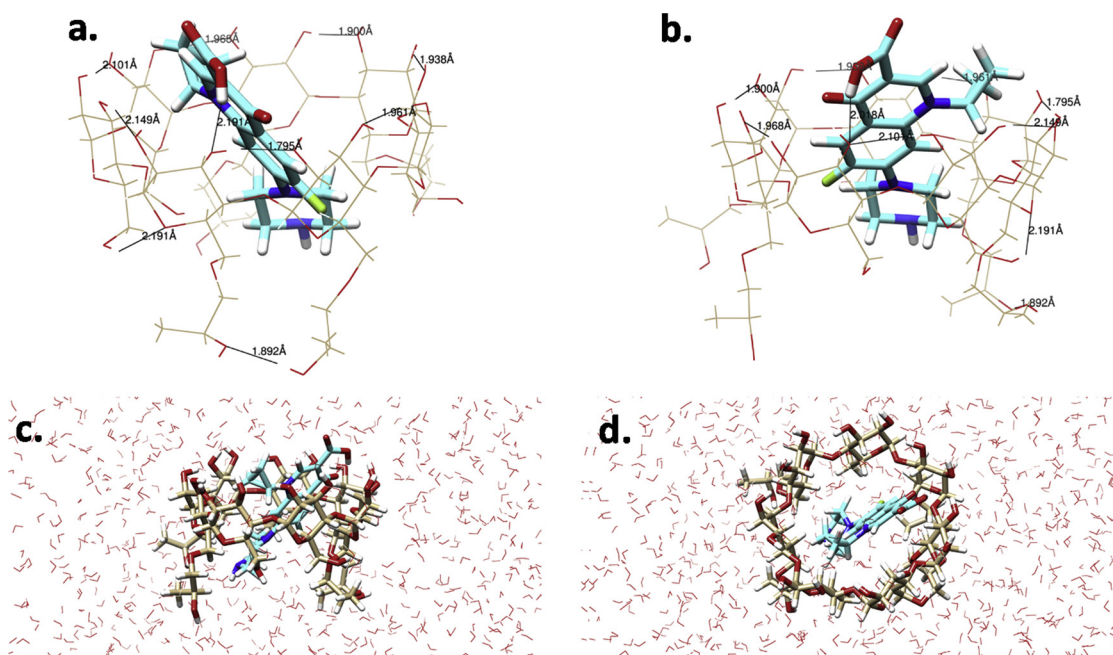
Fig. 2. The side views of the best structures gathered from docking calculations. These two structures (a, b) have similar estimated binding free energies of -5.0 kcal/mol and -5.32 kcal/mol, respectively. MD calculations have been carried out using the structure given in a, as an initial structure. The intermolecular and intramolecular hydrogen bond lengths are also given. (c) Initial structure of MD calculation gathered from docking study, (d) the equilibrated structure at 30 °C within bulk water environment.

carboxyl moiety of CIP has one hydrogen bond with one of the H donor moieties of HPβCD cavity. In both docked structures, the carboxyl moiety of CIP has been found to stay out of HPβCD cavity. Yet, piperazinyl moiety of CIP has tendency to stay towards in HPβCD cavity. The docked structure having ΔG_{bind} of -5.00 kcal/mol has been utilized as initial structure for subsequent MD calculations as given in Fig. 2c.

3.1.2. Molecular dynamics results

We have carried out 30 ns MD calculations at 30 °C by using the one of the best poses of docking study as an initial structure to elucidate thermodynamics of CIP/HPβCD-IC formation. The conformation of host-guest molecule embedded in bulk water environment evolves during 30 ns of MD. GMx cluster tool has been used to cluster similar structures within 2 Å RMSD cut-off along the 30 ns simulation time. Based on the clustering algorithm, we have identified 48 different CD-IC structures along the total trajectory. We have considered the most prevailing structure having the probability of 41% among the other structures as the equilibrium state structure of CD-IC for examining the details of inclusion process. In general, we have seen that the hydrophobic backbone of the CIP is embedded within the HPβCD cavity during 30 ns simulation as shown in Fig. 2d. Nevertheless, CIP has showed different inclusion depths and alignments with respect to the HPβCD axis. In addition, the distance between center of masses of CIP and HPβCD changes at the average of 5 Å for last 15 ns of MD. The carboxyl moiety of CIP remained exposed to water molecules upon IC formation due to being hydrophilic.

It is known that CD-IC formation process is mostly driven by non-bonding interactions such as polar and van der Waals interactions. Considering the equilibrated structure of CD-IC, the evolution of number of hydrogen bonds between host and guest molecules has been determined (Fig. 3b). Moreover, hydrogen bonds formed between CIP and nearby water molecules has been identified (Fig. 3a). The moiety of CIP residing in the cavity of HPβCD has consistent one hydrogen bond with the cavity of HPβCD. It is a fact that hydrogen bonds are not purely electrostatic character. However, the existence of relatively a few numbers of hydrogen bonds between CIP and HPβCD might explain the lower contribution of electrostatic energy to ΔG_{bind} given in Table 1.

However, carboxyl moiety of CIP has shown to have approximately four hydrogen bonds with nearby water molecules. The number of hydrogen bonds with nearby water molecules changes from earlier course of MD as given in Fig. 3c–d. This rearrangement of nearby water molecules plays an important role in the complexation thermodynamics, which is the onset of positive TΔS. Moreover, we have estimated the thermodynamic quantities that cooperate and contribute to the IC formation by means of MM-PBSA method. All interaction components and association constant K_{bind} are given in Table 1. Interestingly, the predicted ΔG_{bind} (-11.33 kcal/mol) is entirely dominated by apolar components (ΔE_{vdw} and $\Delta G_{nonpolar}$). The biggest interaction contribution is ΔE_{vdw} with a value of -19.29 kcal/mol, suggesting that van der Waals interaction is the driving force to form CD-IC. The lower contribution from $\Delta E_{electrostatic}$ may explain the fewer number of hydrogen bonds observed between host and guest molecule. Because $\Delta E_{electrostatic}$ contribution is only calculated for host and guest molecule in MM-PBSA method. Since $\Delta G_{nonpolar}$ is negative, which is typical example of the hydrophobic effect, this suggests that desolvation might occur during CD-IC formation. This possible dehydration of HPβCD cavity upon complexation results in entropic gain, which is supported by positive TΔS value in Table 1. Therefore, the ultimate stability of the CD-IC has enhanced because of this entropic gain. However, the entropic gain cannot cancel the accompanying enthalpy loss, which is as high as -12.13 kcal/mol. The association constant, K_{bind}, is a key indicator to describe the binding affinity, which can be determined both experimentally and computationally. K_{bind} has been calculated for CD-IC by using Eq. (6) and is found to be 1.48×10^8 supporting favorable CD-IC formation within the accuracy of MM-PBSA method.

3.2. Phase solubility of CIP/HPβCD-IC

Phase solubility diagram of CIP/HPβCD system is given in Figure S1. Here, excess amount of CIP was added to the aqueous CD solutions, whose concentration is gradually increasing from 0 to 6 mM. As seen from the diagram, the solubility of CIP improved in a linear fashion up to 6 mM of CD concentration. Since the molar ratio of CIP to HPβCD is 1:1 in the complex that synthesized, phase solubility results support the
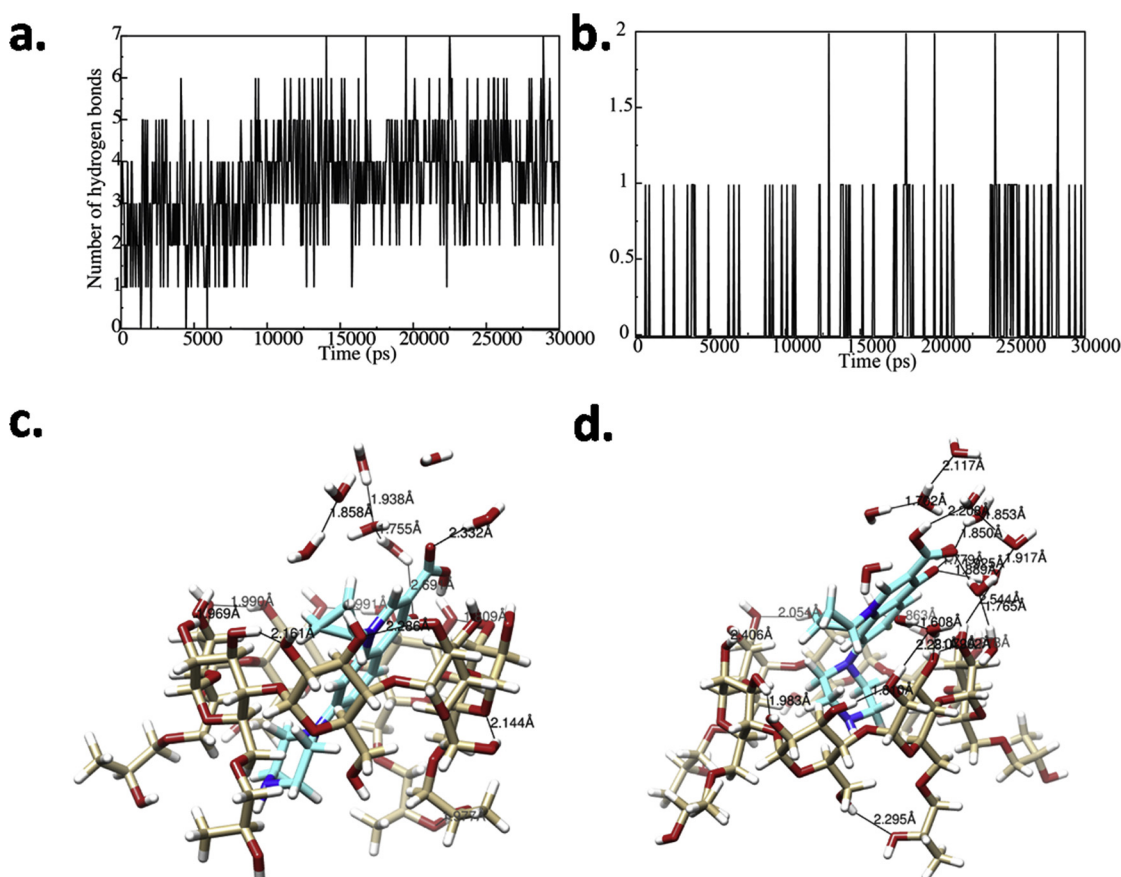
Fig. 3. The variation of number of hydrogen bonds during 30 ns MD between (a) CIP and nearby water molecules, (b) CIP and HPβCD. The hydrogen bonds and corresponding bond lengths are given for (c) the initial state of CD-IC at the beginning of the MD study, (d) the equilibrated state of. CD-IC.

formation of 1:1 complex as well other than showing the solubility improvement compared to the free CIP.

3.3. The molar ratio of CIP/HPβCD-IC

The molar ratio of CIP and HPβCD in CIP/HPβCD-IC was calculated based on the integration of the NMR peaks of each molecule (Figure S2). The integration of the peaks of CIP at 1.17–1.30 ppm [39] in the NMR spectra was proportioned to the integration of the peak of HPβCD at 1.00 ppm. So, the molar ratio of CIP to HPβCD was determined to be 0.75:1.00 in CIP/HPβCD-IC. Therefore, ^{1}H-NMR results confirm that most of the CIP was preserved in the structure even though the applied method for detecting CIP and HPβCD includes filtration of the solution before the measurement.

3.4. Structural characterization of CIP/HPβCD-IC and nanofibers

Structural characterization of CIP, HPβCD, and CIP/HPβCD-IC was carried out by FTIR (Figure S3) and XRD (Fig. 4a). The characteristic peaks of CIP appeared at 3429 cm^{-1} (OH stretching vibration and intermolecular hydrogen bonding) [23,40], 3041 cm^{-1} (aromatic C–H stretching vibration) [23,40], 2850 cm^{-1} (aliphatic C–H stretching vibration) [40], 1614 cm^{-1} (quinolones) [40], 1496 cm^{-1} (C–O

vibration) [40], 1285 cm^{-1} (OH bending vibration of carboxylic acid) [23,40] and 1030 cm^{-1} (C–F stretching) [23,40]. Absorption peaks of CD was observed at 3408 cm^{-1} (OH stretching), 2933 cm^{-1} (C–H stretching), 1645 cm^{-1} (H−OH bending), 1149 cm^{-1} (C–O–C glycosidic antisymmetric stretching vibration), 1071 cm^{-1} (C–O stretching vibration), 1030 cm^{-1} (C–O stretching vibration). The peaks of CIP at the wavenumber of 3429 cm^{-1}, 3041 cm^{-1}, 2850 cm^{-1}, and 1030 cm^{-1} was masked by the peaks of CDs in the FTIR spectra of CIP/HPβCD-IC, whereas the intensity of the peaks at 1614 cm^{-1}, 1496 cm^{-1}, and 1285 cm^{-1} reduced and, these peaks become broader compared to peaks in FTIR of CIP. The most important peak shifting among CIP peaks was the shifting of the peak at 1614 cm^{-1}, which was assigned to quinolones in the molecule, to 1624 cm^{-1}. Additionally, the peak at 1285 cm^{-1} shifted slightly to 1292 cm^{-1}, which shows the presence of an interaction between carboxyl group of CIP and CD cavity. On the other hand, the peak of CD at 1645 cm^{-1} has shifted to 1718 cm^{-1} in the FTIR of CIP/HPβCD-IC. Therefore, there is an interaction between CIP and HPβCD and it was also concluded that CIP inserted to the cavity of CD from the quinolones group and this result is consistent with the modeling study.

CIP has XRD pattern with sharp crystalline peaks, whereas XRD pattern of HPβCD is amorphous. Due to the separation of CIP molecules from each other after they were included in the cavity of HPβCD cause

Table 1

Contributions to binding free energy for CIP/HPBCD-IC (1:1) calculated using MM-PBSA method [37] at 30 °C, considering the most favorable and prevalent orientation during MD snapshots. All values are given in kcal/mol, except K_{bind}.

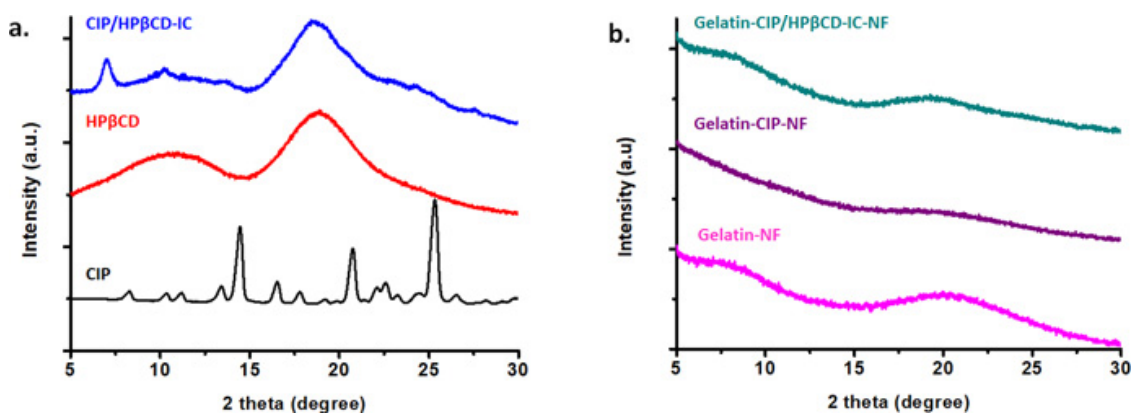| ΔE_{vdw}	$\Delta E_{electrostatic}$	ΔG_{polar}	$\Delta G_{nonpolar}$	$T\Delta S$	ΔH	ΔG	K_{bind}
−19.29	−0.57	10.01	−2,27	0.79	−12.13	−11.33	1.48×10^8

Fig. 4. XRD patterns of (a) CIP, HPβCD, and CIP/HPβCD-IC; (b) gelatin-NF, gelatin-CIP-NF, and gelatin-CIP/HPβCD-IC-NF.

the crystalline peaks of CIP to disappear. In addition, the peaks observed at ˜7° and 10° in the XRD pattern of CIP/HPβCD-IC shows the formation of new crystals after the complexation. As a result, disappearance of crystalline CIP peaks and appearance of new peaks support the successful formation of complex between CIP and HPβCD.

The crystallinity of gelatin-NF, gelatin-CIP-NF, and gelatin-CIP/HPβCD-IC-NF was also investigated, and the results are displayed in Fig. 4b. Similar with the gelatin polymer, gelatin-NF has an amorphous structure with an amorphous diffraction peak. It is known that small crystalline molecules cannot form crystalline aggregates when they are encapsulated in electrospun nanofibers because of the rapid evaporation of solvent during the electrospinning. So, the crystalline peaks of CIP do not exist in the XRD pattern of gelatin-CIP-NF [13]. Gelatin-CIP/HPβCD-IC-NF also exhibited amorphous structure in the XRD pattern due to the amorphous distribution of CIP/HPβCD-IC in gelatin nanofibers [6].

3.5. Thermal characterization of CIP/HPβCD-IC and nanofibers

TGA was the method used to characterize the thermal properties of CIP, HPβCD, and CIP/HPβCD-IC as given in Fig. 5a; and gelatin-NF, gelatin-CIP-NF, and gelatin-CIP/HPβCD-IC-NF as shown in Fig. 5b. HPβCD has two steps of weight loss, first one which is below 100 °C attributed to the water loss in the cavity, whereas the second one shows the main decomposition of HPβCD between 300 °C and 425 °C. The thermal degradation of CIP started at around 270 °C and ended at around 400 °C. CIP/HPβCD-IC, which is a compound composed of HPβCD and CIP, exhibited two distinct weight losses at 25–145 °C and 275–425 °C. Therefore, the thermal stability of CIP slightly improved with the non-covalent interaction, namely inclusion complex formation with HPβCD. Since the thermal degradation of HPβCD and CIP are

overlapping, we were not able to determine amount of each component from TGA results.

Gelatin-NF exhibited two weight losses before 100 °C and after 250 °C, which corresponds to thermal degradation of gelatin. Addition of CIP (gelatin-CIP-NF) did not improve the thermal stability of gelatin-NF as expected. In addition, the amount of CIP could not be calculated from the graph due to the similar thermal degradation profiles of CIP and gelatin. For gelatin-CIP/HPβCD-IC-NF, two steps of weight losses were seen. The weight losses were before 100 °C and after 200 °C. However, since the thermal degradation of all compounds were in the similar temperature ranges, the amounts cannot be calculated.

3.6. Morphology analyses of nanofibers

The morphology of gelatin-NF, gelatin-CIP-NF, and gelatin-CIP/HPβCD-IC-NF was scanned by SEM (Fig. 6a–c). In addition to the bead-free morphology, average fiber diameter (AFD) of gelatin-NF, gelatin-CIP-NF, and gelatin-CIP/HPβCD-IC-NF were calculated as 80 ± 25 nm, 80 ± 15 nm, and 90 ± 20 nm, respectively. The fiber diameters are reported as the average ± standard deviation and 100 fibers were analysed for each sample. The photographs of the nanofibers were also given as insets in Fig. 6a–c and show the free-standing and easily handled feature of nanofibers produced.

3.7. Dissolution of nanofibers

Electrospun nanofibers have potential to be used as carriers for hydrophobic drugs as a fast-dissolving drug delivery system. This unique property of nanofibers can be attributed to not only the high surface area to volume ratio of nanofibers but also the ability of electrospinning technique to transform crystalline small molecules to
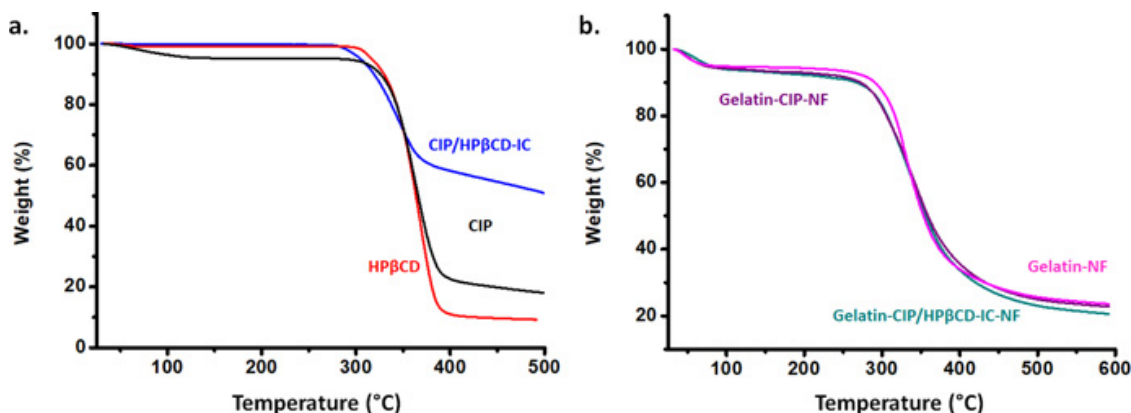

Fig. 5. TGA thermograms of (a) CIP, HPβCD, and CIP/HPβCD-IC; (b) gelatin-NF, gelatin-CIP-NF, and gelatin-CIP/HPβCD-IC-NF.
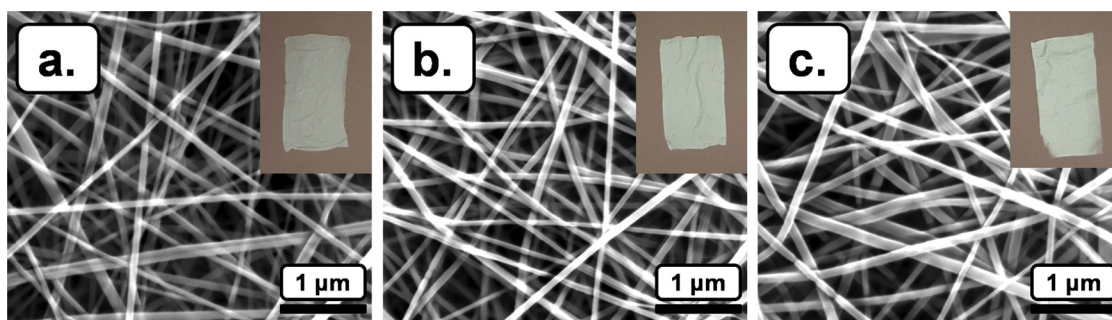
Fig. 6. SEM images and photographs (given as insets) of (a) gelatin-NF, (b) gelatin-CIP-NF, and (c) gelatin-CIP/HPβCD-IC-NF.
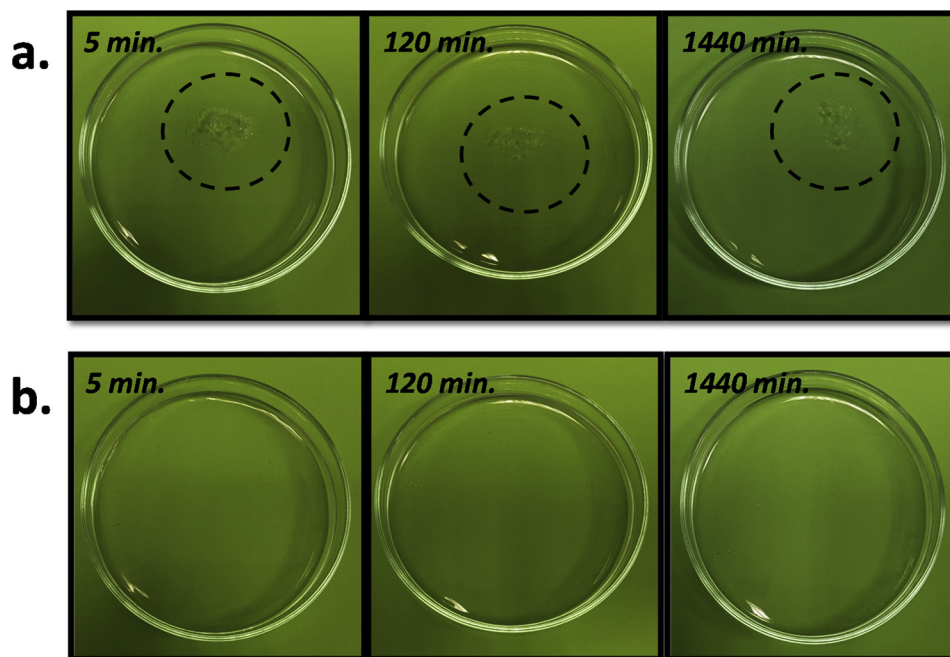

Fig. 7. The photographs of 10 mg of (a) gelatin-CIP-NF and (b) gelatin-CIP/HPβCD-IC-NF, which were immersed in 30 mL of water for 5, 120, and 1440 min.

amorphous molecules due to the rapid evaporation of the solvent. Since high surface area of the carrier increases the contact area with the water and amorphous physical state of drug eliminates the barrier, drug is released into the medium easily.

The dissolution of gelatin-CIP-NF (Supporting video 1) and gelatin-CIP/HPβCD-IC-NF (Supporting video 2) were recorded up to 45 s and the photographs are shown at 5, 120, and 1440 min (Fig. 7a–b). Gelatin-CIP-NF was not able to dissolve even in 1440 min and it is worth mentioning that the nanofibrous mat turns into a transparent material in 30 s. On the contrary, gelatin-CIP/HPβCD-IC-NF completely dissolved in 2–3 s. This is most likely due to the solubility improvement of CIP by the formation of the complex (Figure S1) and enhanced wettability of the mat by the presence of HPβCD. Quite high hydrophilicity of HPβCD facilitates the penetration of water into the pores [27], in addition to the solubility of gelatin in aqueous solution, amorphous distribution of CIP/HPβCD-IC in the nanofibers (Fig. 4b), and high surface are of the nanofibers (90 ± 20 nm) (Fig. 6c).

4. Conclusion

CIP/HPβCD-IC was encapsulated in gelatin nanofibers having the AFD of ~90 nm produced by electrospinning. Computational modeling studies showed that hydrophobic moiety (piperazinyl) in CIP molecule inserted in the cavity, whereas hydrophilic moiety (carboxylic acid) of the molecule is facing outward the cavity. This result is also consistent

with the FTIR results in which the highest shift observed in the peaks of hydrophobic moiety. It was also shown that van der Waals forces are the most importing driving forces for the complexation from computational modeling studies. Experimental studies such as phase solubility, FTIR, and XRD supported the formation of CD-IC as well. The molar ratio of CIP:HPβCD was calculated to be 0.75:1.00 from ^{1}H-NMR. A clear improvement in the solubility of CIP, when it is included in the cavity of HPβCD, was observed from the phase solubility diagram. Therefore, CIP/HPβCD-IC encapsulated gelatin nanofibers exhibited quick dissolution in 3 s in contrast to only CIP encapsulated gelatin nanofibers, which cannot completely dissolve even in 1440 min. The fast disintegration of CIP/HPβCD-IC encapsulated gelatin nanofibers compared to only CIP encapsulated gelatin nanofibers is most likely due to the solubility and wettability enhancement provided by the CD in the mat. As a conclusion, this study might open a new area of investigation for the drug delivery systems that needs to be dissolved quickly.

Appendix A. Supplementary data

Supplementary material related to this article can be found, in the online version, at doi:https://doi.org/10.1016/j.colsurfb.2019.02.059.

References

[1] S. Thenmozhi, N. Dharmaraj, K. Kadirvelu, H.Y. Kim, Electrospun nanofibers: new generation materials for advanced applications, Mater. Sci. Eng. B 217 (2017) 36–48.

[2] B. Ghafoor, A. Aleem, M.N. Ali, M. Mir, Review of the fabrication techniques and applications of polymeric electrospun nanofibers for drug delivery systems, J. Drug Deliv. Sci. Technol. (2018).

[3] S.P. Miguel, D.R. Figueira, D. Simões, M.P. Ribeiro, P. Coutinho, P. Ferreira, I.J. Correia, Electrospun polymeric nanofibres as wound dressings: a review, Colloids Surf. B Biointerfaces 169 (2018) 60–71.

[4] T. Uyar, E. Kny (Eds.), Electrospun Materials for Tissue Engineering and Biomedical Applications: Research, Design and Commercialization, Woodhead Publishing, 2017.

[5] Z. Aytac, T. Uyar, Antioxidant activity and photostability of α-tocopherol/β-cyclodextrin inclusion complex encapsulated electrospun polycaprolactone nanofibers, Eur. Polym. J. 79 (2016) 140–149.

[6] Z. Aytac, T. Uyar, Core-shell nanofibers of curcumin/cyclodextrin inclusion complex and polylactic acid: enhanced water solubility and slow release of curcumin, Int. J. Pharm. 518 (1–2) (2017) 177–184.

[7] Z. Aytac, S.Y. Dogan, T. Tekinay, T. Uyar, Release and antibacterial activity of allyl isothiocyanate/β-cyclodextrin complex encapsulated in electrospun nanofibers, Colloids Surf. B Biointerfaces 120 (2014) 125–131.

[8] Z. Aytac, S. Ipek, E. Durgun, T. Tekinay, T. Uyar, Antibacterial electrospun zein nanofibrous web encapsulating thymol/cyclodextrin-inclusion complex for food packaging, Food Chem. 233 (2017) 117–124.

[9] Z. Aytac, S. Ipek, E. Durgun, T. Uyar, Antioxidant electrospun zein nanofibrous web encapsulating quercetin/cyclodextrin inclusion complex, J. Mater. Sci. 53 (2) (2018) 1527–1539.

[10] Z. Aytac, N.O.S. Keskin, T. Tekinay, T. Uyar, Antioxidant α-tocopherol/γ-cyclodextrin–inclusion complex encapsulated poly (lactic acid) electrospun nanofibrous web for food packaging, J. Appl. Polym. Sci. 134 (21) (2017).

[11] Z. Aytac, S.I. Kusku, E. Durgun, T. Uyar, Encapsulation of gallic acid/cyclodextrin inclusion complex in electrospun polylactic acid nanofibers: release behavior and antioxidant activity of gallic acid, Mater. Sci. Eng. C 63 (2016) 231–239.

[12] Z. Aytac, S.I. Kusku, E. Durgun, T. Uyar, Quercetin/β-cyclodextrin inclusion complex embedded nanofibres: slow release and high solubility, Food Chem. 197 (2016) 864–871.

[13] Z. Aytac, H.S. Sen, E. Durgun, T. Uyar, Sulfisoxazole/cyclodextrin inclusion complex incorporated in electrospun hydroxypropyl cellulose nanofibers as drug delivery system, Colloids Surf. B Biointerfaces 128 (2015) 331–338.

[14] T. Uyar, J. Hacaloglu, F. Besenbacher, Electrospun polyethylene oxide (PEO) nanofibers containing cyclodextrin inclusion complex, J. Nanosci. Nanotechnol. 11 (5) (2011) 3949–3958.

[15] M.E. Davis, M.E. Brewster, Cyclodextrin-based pharmaceutics: past, present and future, Nat. Rev. Drug Discov. 3 (12) (2004) 1023.

[16] O. Adeoye, H. Cabral-Marques, Cyclodextrin nanosystems in oral drug delivery: a mini review, Int. J. Pharm. 531 (2) (2017) 521–531.

[17] T. Loftsson, D. Duchene, Cyclodextrins and their pharmaceutical applications, Int. J. Pharm. 329 (1-2) (2007) 1–11.

[18] K.S. Aithal, N. Udupa, Physicochemical study of ciprofloxacin with β-Cyclodextrin, Pharm. Pharmacol. Commun. 2 (10) (1996) 451–455.

[19] H. Li, J. Sun, Y. Wang, X. Sui, L. Sun, J. Zhang, Z. He, Structure-based in silico model profiles the binding constant of poorly soluble drugs with β-cyclodextrin, Eur. J. Pharm. Sci. 42 (1–2) (2011) 55–64.

[20] N. Rajendiran, T. Mohandoss, J. Thulasidhasan, Encapsulation of ciprofloxacin, sparfloxacin, and ofloxacin drugs with α-and β-cyclodextrins: spectral and molecular modelling studies, Phys. Chem. Liquids 54 (2) (2016) 193–212.

[21] B. Blanco-Fernandez, M. Lopez-Viota, A. Concheiro, C. Alvarez-Lorenzo, Synergistic performance of cyclodextrin–agar hydrogels for ciprofloxacin delivery and antimicrobial effect, Carbohydr. Polym. 85 (4) (2011) 765–774.

[22] J. Chao, D. Meng, J. Li, H. Xu, S. Huang, Preparation and study on the novel solid inclusion complex of ciprofloxacin with HP-β-cyclodextrin, Spectrochim. Acta A. Mol. Biomol. Spectrosc. 60 (3) (2004) 729–734.

[23] S. Masoumi, S. Amiri, S.H. Bahrami, PCL-based nanofibers loaded with ciprofloxacin/cyclodextrin containers, J. Text. Inst. 109 (8) (2018) 1044–1053.

[24] U.E. Illangakoon, H. Gill, G.C. Shearman, M. Parhizkar, S. Mahalingam, N.P. Chatterton, G.R. Williams, Fast dissolving paracetamol/caffeine nanofibers prepared by electrospinning, Int. J. Pharm. 477 (1–2) (2014) 369–379.

[25] Y.H. Wu, D.G. Yu, X.Y. Li, A.H. Diao, U.E. Illangakoon, G.R. Williams, Fast-dissolving sweet sedative nanofiber membranes, J. Mater. Sci. 50 (10) (2015) 3604–3613.

[26] W. Samprasit, P. Akkaramongkolporn, T. Ngawhirunpat, T. Rojanarata, R. Kaomongkolgit, P. Opanasopit, Fast releasing oral electrospun PVP/CD nanofiber mats of taste-masked meloxicam, Int. J. Pharm. 487 (1–2) (2015) 213–222.

[27] W. Samprasit, P. Akkaramongkolporn, R. Kaomongkolgit, P. Opanasopit, Cyclodextrin-based oral dissolving films formulation of taste-masked meloxicam, Pharm. Dev. Technol. 23 (5) (2018) 530–539.

[28] G.M. Morris, R. Huey, W. Lindstrom, M.F. Sanner, R.K. Belew, D.S. Goodsell, A.J. Olson, AutoDock4 and AutoDockTools4: Automated docking with selective receptor flexibility, J. Comput. Chem. 30 (16) (2009) 2785–2791.

[29] E.F. Pettersen, T.D. Goddard, C.C. Huang, G.S. Couch, D.M. Greenblatt, E.C. Meng, T.E. Ferrin, UCSF Chimera—a visualization system for exploratory research and analysis, J. Comput. Chem. 25 (13) (2004) 1605–1612.

[30] S. Jo, T. Kim, V.G. Iyer, W. Im, CHARMM-GUI: a web-based graphical user interface for CHARMM, J. Comput. Chem. 29 (11) (2008) 1859–1865.

[31] J. Lee, X. Cheng, J.M. Swails, M.S. Yeom, P.K. Eastman, J.A. Lemkul, et al., CHARMM-GUI input generator for NAMD, GROMACS, AMBER, OpenMM, and CHARMM/OpenMM simulations using the CHARMM/additive force field, J. Chem. Theory Comput. 12 (1) (2015) 405–413.

[32] K. Vanommeslaeghe, E. Hatcher, C. Acharya, S. Kundu, S. Zhong, J. Shim, et al., CHARMM general force field: a force field for drug-like molecules compatible with the CHARMM all-atom additive biological force fields, J. Comput. Chem. 31 (4) (2010) 671–690.

[33] M.J. Abraham, T. Murtola, R. Schulz, S. Páll, J.C. Smith, B. Hess, E. Lindahl, GROMACS: High performance molecular simulations through multi-level parallelism from laptops to supercomputers, SoftwareX 1 (2015) 19–25.

[34] D.J. Evans, B.L. Holian, The nose–Hoover thermostat, J. Chem. Phys. 83 (1985) 4069–4074.

[35] T. Darden, D. York, L. Pedersen, Particle mesh Ewald: an N· log (N) method for Ewald sums in large systems, J. Chem. Phys. 98 (12) (1993) 10089–10092.

[36] B. Hess, H. Bekker, H.J. Berendsen, J.G. Fraaije, LINCS: a linear constraint solver for molecular simulations, J. Comput. Chem. 18 (12) (1997) 1463–1472.

[37] I. Beà, M.G. Gotsev, P.M. Ivanov, C. Jaime, P.A. Kollman, Chelate effect in cyclodextrin dimers: a computational (MD, MM/PBSA, and MM/GBSA) study, J. Org. Chem. 71 (5) (2006) 2056–2063.

[38] R. Kumari, R. Kumar, Open Source Drug Discovery Consortium, A. Lynn, g_mmpbsa-A GROMACS tool for high-throughput MM-PBSA calculations, J. Chem. Inf. Model. 54 (7) (2014) 1951–1962.

[39] A. Zieba, A. Maslankiewicz, J. Sitkowski, Spectral Assignments and Reference Data-¹H, ¹³C and ¹⁵N NMR spectra of ciprofloxacin, Magn. Reson. Chem. 42 (2004) 903–904.

[40] S. Sahoo, C.K. Chakraborti, P.K. Behera, FTIR and Raman spectroscopic investigations of a controlled release Ciprofloxacin/Carbopol940 mucoadhesive suspension, Asian J. Pharm. Clin. Res 5 (1) (2012) 125–130.